Available online at www.sciencedirect.com
SCIENCE DIRECT
Polymer 47 (2006) 4773–4780
polymer
www.elsevier.com/locate/polymer

Morphology, structure and properties of a poly(1-butene)/montmorillonite nanocomposite

Valerio Causin [a,*], Carla Marega [a], Antonio Marigo [a], Giuseppe Ferrara [b], Gulnaz Idiyatullina [b], Fabiana Fantinel [b]

[a] *INSTM Research Unit, Dipartimento di Scienze Chimiche, Università di Padova, via Marzolo 1, 35131 Padova, Italy*
[b] *Basell Poliolefine Italia SpA, Centro Ricerche 'Giulio Natta', P.le Donegani 12, 44100 Ferrara, Italy*

Received 29 September 2005; received in revised form 20 December 2005; accepted 21 April 2006
Available online 15 May 2006

Abstract

A specifically formulated nanocomposite based on isotactic poly(1-butene) (PB) and montmorillonite was studied, by wide angle X-ray diffraction (WAXD), small angle X-ray scattering (SAXS), transmission electron microscopy (TEM) and polarized light optical microscopy, investigating the polymorphism of the polymer, and examining the interaction between PB and the silicate. Montmorillonite was found to disrupt the ordered morphology of the polymer, determining a dramatic increase in the rate of the II→I phase transition. Interaction between polymer and clay was studied by TEM and SAXS also under a quantitative point of view. A significant enhancement of physical–mechanical properties was observed, even though exfoliation did not occur, but just a slight intercalation and a reduction in the size of tactoids.

Keywords: Nanocomposites; Polybutene; Small angle X-ray scattering

1. Introduction

Isotactic poly(1-butene), first synthesized by Natta and co-workers [1] in 1954, is a polymer with a number of attractive properties that distinguish it from the most common polyolefins like isotactic polypropylene and polyethylene. It exhibits advantages over other polyolefins in toughness, tear strength, flexibility, creep, stress cracking resistance, impact resistance, abrasion resistance and high-temperature resistance. This polymer can crystallize in several polymorphs, but only tetragonal phase II and hexagonal phase I are of practical interest. Form II, in which the conformation of the chains is a 11_3 helix, characterized by a tetragonal unit cell, is kinetically favored when the polymer is crystallized from the melt. At room temperature this modification is metastable and it converts to phase I, with 3_1 helices organized in a hexagonal unit cell [2,3]. The II→I transformation brings about important structural changes, that are reflected in considerable improvements in many physical–mechanical properties among, which density, crystallinity, hardness, rigidity, stiffness and tensile strength [4–6]. The II→I phase transition requires several days to be completed [5,7–10] and this slow kinetics is the principal reason why the commercial development of poly(1-butene) has been much delayed. A great deal of research has thus been oriented towards finding solutions to accelerate the transition. Addition of layered silicate fillers, such as montmorillonite clay, to prepare nanocomposites is likely to improve the mechanical performance of poly(1-butene) and to have a significant influence on the kinetics of the II→I transition [11–13]. Wanjale and Jog [11,12] recently studied nanocomposites based on PB and organoclay prepared by melt-blending. They observed that formation of an intercalated clay network produced significant changes in the crystallization behavior and accelerated the II→I phase transition. Moreover, addition of a clay nanofiller brought about a different response to stress during tensile straining [13]. In the present work, the same approach was adopted, but the formulation was optimized with a maleated polypropylene-based compatibilizer that improved the polymer–clay interaction. This permitted a further improvement especially in the rate and extent of the II→I phase transition. The purpose of this paper was to prepare and characterize the structure and morphology of this particular formulation of a poly(1-butene)/montmorillonite composite, studying how the addition of filler influences the kinetics of the II→I transition and physical–mechanical properties.

* Corresponding author. Tel.: +39 049 8275153; fax: +39 049 8275161.
E-mail address: valerio.causin@unipd.it (V. Causin).

0032-3861/$ - see front matter © 2006 Elsevier Ltd. All rights reserved.
doi:10.1016/j.polymer.2006.04.035

Wide angle X-ray diffraction (WAXD), small angle X-ray scattering (SAXS), polarized light optical microscopy (PLOM) and transmission electron microscopy (TEM) were used to characterize the structure and morphology of the samples. Thermogravimetry, tensile, flexural and impact testing were the techniques employed in the physical mechanical characterization.

2. Experimental

2.1. Samples and sample preparation

A commercially available grade of poly(1-butene) homopolymer, PB0300M ($\bar{M}_w = 284196$, $\bar{M}_w/\bar{M}_n = 3.6$), produced by Basell Polyolefins S.p.A. was used in this work. A 5% content of Cloisite 15-A (Southern Clay Products) was added. Cloisite 15-A is montmorillonite ion-exchanged with octadecylammonium ions. A 7% content of HIFAX KA807 maleated PP (Basell Polyolefins) was employed as a compatibilizing agent. The components were mixed in a reciprocating single screw extruder, Buss MDK 70. The extrusion average temperature was 180 °C, the residence time was 80 s. The profile of the employed screw was obtained by that normally used with talc by the elimination of restriction rings to optimize distributive mixing and residence time [14].

The obtained pellets were subsequently processed by injection molding in accordance with ISO 294-1 or ISO 294-3. Test specimens were conditioned in accordance with ISO 291 for at least 40 h at (23 ± 2) °C and (50 ± 5)% relative humidity. Neat polybutene (PB) was subjected to the same thermo-mechanical history of the composite PB-M.

The study of the II → I transition was carried out on both PB and the composite PB-M by melting aliquots of the samples between two aluminum plates in a press at 170 °C for 20 min and then letting the specimens cool down to room temperature at a rate of 10 °C/min. Experiments were performed in which samples were quenched in ice after melting. Results in both cases were exactly analogous, so in this paper results will be presented of samples slowly cooled from the melt.

2.2. Wide angle X-ray diffraction

WAXD patterns were recorded in the diffraction angular range 1.5–40° 2θ by a Philips X'Pert PRO diffractometer, working in the reflection geometry and equipped with a graphite monochromator on the diffracted beam (Cu K_α radiation). Transmission patterns were also recorded in the diffraction range 5–40° 2θ by a diffractometer GD 2000 (Ital Structures) working in a Seeman–Bohlin geometry and with a quartz crystal monochromator on the primary beam (Cu $K_{\alpha 1}$ radiation). Results were the same either in the transmission and reflection mode, so it was concluded that no difference in structure and morphology existed in the samples between the bulk and the surface. The data presented in this paper were gathered in the reflection geometry. The application of the least-squares fit procedure elaborated by Hindeleh and Johnson [15] gave the degree of crystallinity by weight, which was then transformed in degree of crystallinity by volume [16] (ϕ_{WAXD}). The phase transition II → I was followed observing the WAXD patterns and estimating the ratio A_t/A_0, where A_t represents the area under the peak at 11.9° 2θ (corresponding to the (200) reflection of phase II) at time t, and A_0 is the area of the same peak just after crystallization from the melt.

2.3. Small angle X-ray scattering

The SAXS patterns of the samples were recorded by an MBraun system, utilizing a Cu K_α radiation from a Philips PW 1830 X-ray generator. The data were collected by a position sensitive detector and they were successively corrected for blank scattering.

Finally, the Lorentz correction was applied: $I_1(s) = 4\pi s^2 I(s)$, where $I_1(s)$ is the one-dimensional scattering function and $I(s)$ the desmeared intensity function, being $s = (2/\lambda)\sin\theta$.

2.4. SAXS data analysis

The evaluation of the SAXS patterns according to some theoretical distribution models [17] was carried out referring to the Hosemann model [18], that assumes the presence of lamellar stacks having an infinite side dimension. This assumption takes into account a monodimensional electron density change along the normal direction to the lamellae.

This method was already employed to describe the clay tactoids in polymer-based nanocomposite systems [14,19] and, in this study, it was applied both to the polymeric lamellar stacks and to the alternation of high-density alumino-silicate layers with low-density regions interposed.

The intensity profile was evaluated as

$$I(s) = I^{I}(s) + I^{II}(s)$$

where:

$$I^{I}(s) = \frac{(\rho_Y - \rho_Z)^2}{4\pi^2 s^2 D} \times \frac{|1 - F_Y|^2(1 - |F_Z|^2) + |1 - F_Z|^2(1 - |F_Y|^2)}{(1 - F_Y F_Z)^2}$$

$$I^{II}(s) = \frac{(\rho_Y - \rho_Z)^2}{2\pi^2 s^2 DN} \times \mathrm{Re}\left\{\frac{F_Z(1 - F_Y)^2(1 - (F_Y F_Z)^N)}{(1 - F_Y F_Z)^2}\right\}$$

In these equations, F_Y and F_Z represent the Fourier transforms of the distribution functions of the high-density (Y) and of the low-density (Z) regions, ρ_Y and ρ_Z are the electron densities of the high and low-density regions, respectively, N is the number of layers (polymeric lamellae or alumino-silicate layers) in the system and D the average long period. A fitting procedure of the calculated one dimensional scattering functions with the experimental ones allows to optimize the values of the high and low-density region thicknesses. Crystallinity (ϕ_{SAXS}) was evaluated as the ratio between the thickness of the high-density (crystalline) regions over the long period $D = Y + Z$.

2.5. Transmission electron microscopy

TEM analysis were performed by a Phillips CM 120. Samples were stained by RuO_4 and cryomicrotomed. Sections about 100 nm thick were obtained and analyzed.

2.6. Polarized light optical microscopy

The spherulitic morphology of PB and PB-M samples were studied with a Leica DM400M polarized light microscope. The samples were placed between a glass slide and a cover slip and were kept at 170 °C for 10 min, to ensure uniform melting and to delete their thermal history. The slide was then transferred to a Mettler FP82HT hot stage set at room temperature. The photomicrographs were taken between cross-polarizers with a Leica DFC280 digital camera.

2.7. Mechanical properties

The flexural modulus (MEF) and elongational properties (stress and elongation at break) were determined in accordance with ISO 178 using an Instron 4301 instrument on the injection molded specimens after 10 min in autoclave at 2000 bars and a conditioning period of 24 h at 23 °C and 50% of humidity. The melt flow rate (MFR) was measured by forcing the melt through a capillary under a dead load at constant temperature (2.16 kg, 190 °C in accordance with ISO-1133).

Impact strength was measured with a Ceast 6545 pendulum type hammer striking a notched specimen with a 0.05 mm notch (ISO 180).

2.8. Thermal analysis

Differential scanning calorimetry measurements were carried out with a model 2920 calorimeter (TA Instruments) operating under N_2 atmosphere. The samples, weighing about 5 mg, were closed in aluminum pans. A heating rate of 10 °C/min up to 150 °C was set in order to observe the polymer melting peak. Indium of high-purity was used for calibrating the DSC temperature and enthalpy scales. Thermogravimetric analysis (TGA) was performed with a TA Instruments SDT 2960 simultaneous TG/DSC system. The scans were recorded at a heating rate of 20 °C/min in a temperature range from 30 to 700 °C. Experiments were done under air and nitrogen atmosphere. The onset of the degradation (T_{onset}) was calculated as the intersection between the starting mass line and the line of maximum gradient tangent to the TG curve, while the end point (T_{offset}) was evaluated as the point of intersection of the minimum gradient tangent following completion of the mass decrease step and the maximum gradient tangent to the TG curve. The temperature correspondent to the maximum of the derivative of the TG curve with respect to temperature was also noted (T_{max}).

3. Results and discussion

Figs. 1 and 2 show some WAXD patterns of the samples, recorded at different aging times during the II→I phase transition. The reflections relative to the tetragonal modification are basically three main peaks at 11.9, 16.9 and 18.4° 2θ, corresponding to the (200), (220) and (301) planes. The hexagonal phase I is characterized by four signals at 9.9, 17.3, 20.2 and 20.5° 2θ, originated by the (110), (300), (220) and (211) planes, respectively [20]. It may be noted that, as a consequence of the phase transition, with increasing time the intensity of the peaks typical of the hexagonal phase I (i.e. (110) at 9.9° 2θ) increases, whereas the intensity of peaks related to the tetragonal phase II (i.e. (200) at 11.9° 2θ) decreases.

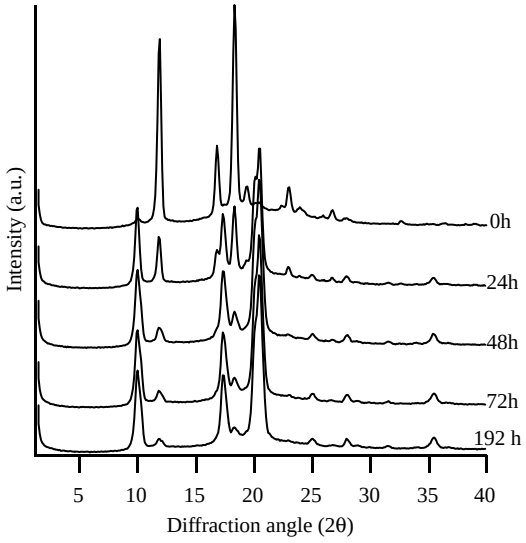

Fig. 1. WAXD patterns of sample PB at different aging times.

A quite striking difference in the polymorphism of the two samples can be noted in the diffractograms taken at the initial time. While in PB almost 100% phase II is detected, in PB-M a relevant amount of phase I co-exists with form II right after the cooling from the melt. Montmorillonite seems then to act as a nucleant for phase I. In their study on the crystallization of poly(1-butene), Kaszonyiova and co-workers found that nucleating agents did not influence the polymorphism, but

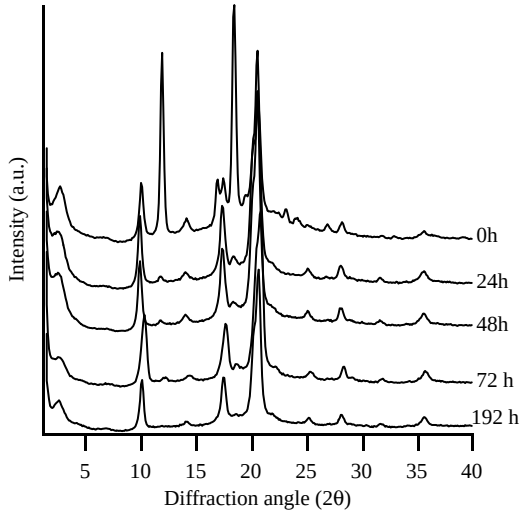

Fig. 2. WAXD patterns of sample PB-M at different aging times.

only the crystallization rate [10]. All the nucleants they considered produced 100% phase II in the as-crystallized samples, and had no effect on the rate of the II→I transformation [10]. The appearance of phase I in the very early stages of the aging process following crystallization from the melt was reported in the case of 1-butene/ethylene copolymers [20,21]. In that instance, two populations of phase II crystals were produced by the crystallization from the melt, differing by structural order and by the amount of constitutional defects incorporated. The more defective form II crystals exhibited a much faster II→I conversion rate than the ordered ones, thus leading to the formation of the I polymorph at very short aging times [20]. A similar situation can be found in sample PB-M. Figs. 3 and 4 show PLOM micrographs of samples PB and PB-M. In the neat polymer, well defined spherulites can be seen (Fig. 3). In the composite, on the contrary, the nucleating effect of montmorillonite is evident: a very large number of small crystallites are formed, without the neatly ordered structure observed in the pure polymer (Fig. 4). The disorder and the nucleation brought about by the addition of montmorillonite was observed also by Wanjale and Jog [11].

The degrees of crystallinity (ϕ_{WAXD}) measured for the two samples from their WAXD patterns reflect their different formulation. As-crystallized PB had a ϕ_{WAXD} of 66%, while this value increased to 76 and 77% if the measure was taken after an aging time of 72 or 192 h, respectively. When PB-M was taken into account, crystallinities were lower than those of the neat polymer: for aging times of 0, 72 and 192 h, ϕ_{WAXD} equaled to 63, 72 and 73%, respectively. This may be due to the addition of non-crystallizable maleated PP oligomer used as a compatibilizing agent that increased the amount of amorphous phase. At the same time, it is well known [11,22–26] that the presence of the clay hinders the formation of ordered crystallites and that it introduces a large number of heterogeneous nuclei of crystallization. This effect is usually detected in the morphology observed by PLOM (Figs. 3 and 4) of spherulites that are much smaller and less perfect in nanocomposites as a consequence of a significant nucleation and a fast crystallization rate that does not allow enough time to

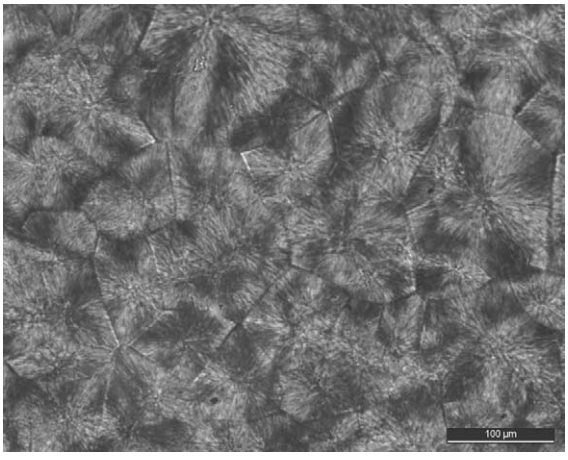

Fig. 3. PLOM micrograph of sample PB. The metric bar corresponds to 100 µm.

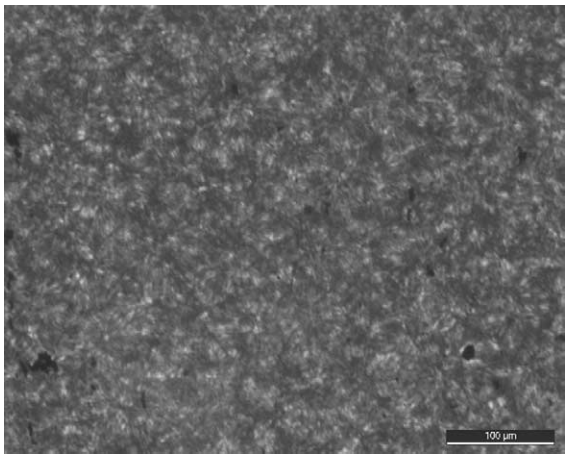

Fig. 4. PLOM micrograph of sample PB. The metric bar corresponds to 100 µm.

attain an ordinate morphology [11,23–25]. Lincoln and co-workers reported that the disturbing effect of clay is carried out at a lamellar level, without altering the overall degree of crystallinity [26]. In the case of the samples examined in this work, a broad distribution of the dimensions of crystallites could be detected also observing the breadth and structure of the DSC melting endotherms (Fig. 5), that is known to depend on the type of crystalline phases and on the distribution of crystallite sizes [27]. Both the DSC traces were obtained on the samples after completion of the II→I phase transition, so the effect of polymorphism on the formation of the shoulder in the PB-M endotherm can be ruled out. The broader and less regular shape of the peak relative to sample PB-M can thus be ascribed to a greater disorder induced by the addition of the clay and of the compatibilizer.

For the quantification of the kinetics of the II→I phase transition, the disappearance of phase II, rather than the increase in phase I, was followed because it is known that, together with the phase transition, a post-crystallization phenomenon takes place, during which part of the amorphous polymer crystallizes in phase I [4,20,28,29]. The ϕ_{WAXD} data presented above indeed confirmed what had been previously reported, i.e. that an increase in crystallinity occurs with aging time, reaching a plateau around 75 h [4].

The percent change of the area of the (200) peak at 11.9° 2θ relative to phase II are reported in Fig. 6 for samples PB and

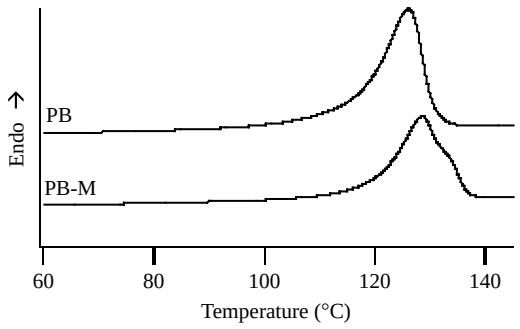

Fig. 5. Melting endotherms of samples PB and PB-M after an aging time of 3 months.

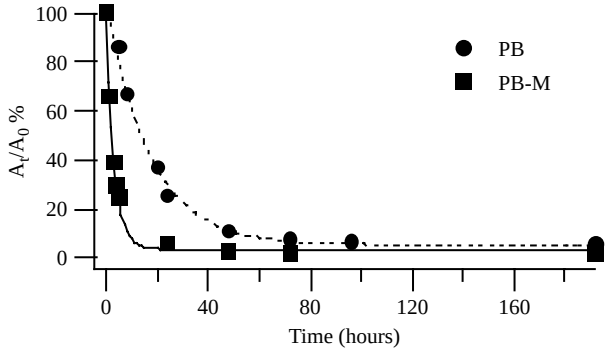

Fig. 6. Percent change, as a function of time, of the (200) peak area in samples PB (●) and PB-M (■). The lines indicate the exponential fitting functions used to determine the half time of transformation.

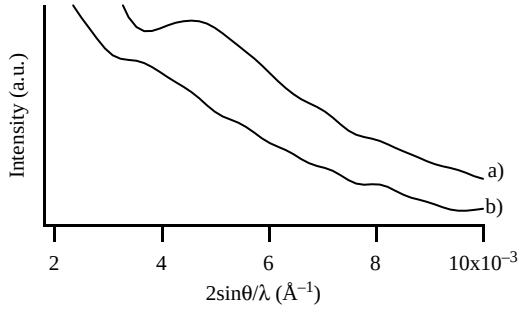

Fig. 7. SAXS patterns of samples (a) PB and (b) PB-M in the polymer lamellar periodicity region.

PB-M. The experimental points were fit by an exponential curve and the half time for the transformation ($t_{½}$) was obtained. As can be seen, the II→I transformation is remarkably faster in PB-M than in PB: when montmorillonite was added, $t_{½}$ equaled 2.2 h, while in neat PB $t_{½}$ was 13.5 h. The phase transition of sample PB-M was also more complete, with a residual (200) peak just 3% the original area, after only 72 h, whereas PB, after 8 days, still contained 6% of phase II. Although the effect of the relevant quantity of compatibilizer present in PB-MA cannot be ruled out, the influence of clay should be deemed preponderant, as shown by the fact that the improvements in performance of PB-based composites could be observed only on the system PB-clay-maleated PP, and not on the blend of PB with just maleated PP [30].

It should be remarked that the same structure and the same behavior in the II→I transformation were observed also if the samples were quenched in ice after melting, instead of being left to cool down at 10 °C/min, and if WAXD spectra were recorded in the transmission mode. This, along with the fact that both PB and PB-M were subjected to the same thermo-mechanical history, permits to rule out the effect of sample preparation and of surface effects (WAXD spectra in the transmission mode sample the whole bulk of the specimen, while its surface is studied by reflection geometry) on the reported behavior.

The study of the effect of montmorillonite on the structure of the polymer matrix was completed by a SAXS investigation. It is well known, and was confirmed by our measurements, that a SAXS signal relative to the lamellar morphology of the polymer is detectable only after a few hours of aging [4,21,31]. This is probably due to two concurrent effects: the slight difference of electronic density between the crystalline and the amorphous phase in form II and the presence of bent lamellae not organized, in the II polymorph, in stacks [4,21,31]. Fig. 7 shows the SAXS patterns of samples PB and PB-M after an aging time of 8 days. It is evident that PB-M displays a much worse SAXS signal than PB. A fitting procedure [17] was applied to these SAXS traces and the morphology of the lamellar stacks was elucidated. Table 1 shows the parameters obtained. PB-M displays a larger thickness of the crystalline layer, probably due to the more complete conversion of phase II into form I. During the transformation, in fact, an elongation of the helical axes occur, with the monomeric unit distance changing from 1.87 Å of phase II to 2.17 Å of phase I [4]. PB-M is characterized by a lower crystallinity than PB, which is principally due to the large thickness of the amorphous layer. This datum, along with the appearance of the SAXS pattern of PB, which is much sharper and neater than that of PB-M, confirms that montmorillonite significantly disrupts the structural order, also at a lamellar level. The role of clay in confining macromolecular chains, inhibiting their mobility and physically hindering the growth of lamellar structures, has been widely reported in the literature [18,23,24,26,27,32]. This effect is clearly visible in TEM micrographs (Fig. 8). The role of clay in interrupting and altering the morphology of polymeric lamellae can be seen, especially if compared with TEM micrographs of neat PB (Fig. 9). Fig. 8(c) shows for example, three black clay layers hampering and dividing neighboring polymeric lamellar stacks. By comparison of Figs. 8(b) and 9(a), taken at the same magnification on samples PB-M and PB, respectively, it can be noted that the density of polymeric lamellar stacks is significantly lower in PB-M, with a preferential aggregation around clay particles. The nucleating effect of clay, the segregation of maleated PP in the amorphous phase and the confinement of macromolecular chains by the nanofiller produced then the alterations of the lamellar stacks observed by SAXS. The nucleation centers of the II→I transition are located on the lamellar distortion points [4,33], so a larger dishomogeneity in the lamellar structure brings about a faster phase transformation.

Table 1
Average thicknesses of the lamellar (Y) and amorphous (Z) layers, long period (D), with their relative distributions (σ_Y/Y, σ_Z/Z and σ_D/D), and degree of crystallinity (ϕ_{SAXS}) of the polymeric lamellar stacks measured by SAXS for samples PB and PB-M

	Y (Å)	Z (Å)	D (Å)	σ_Y/Y	σ_Z/Z	σ_D/D	ϕ_{SAXS}
PB	163	50	213	0.34	0.34	0.28	76
PB-M	178	84	262	0.31	0.31	0.23	68

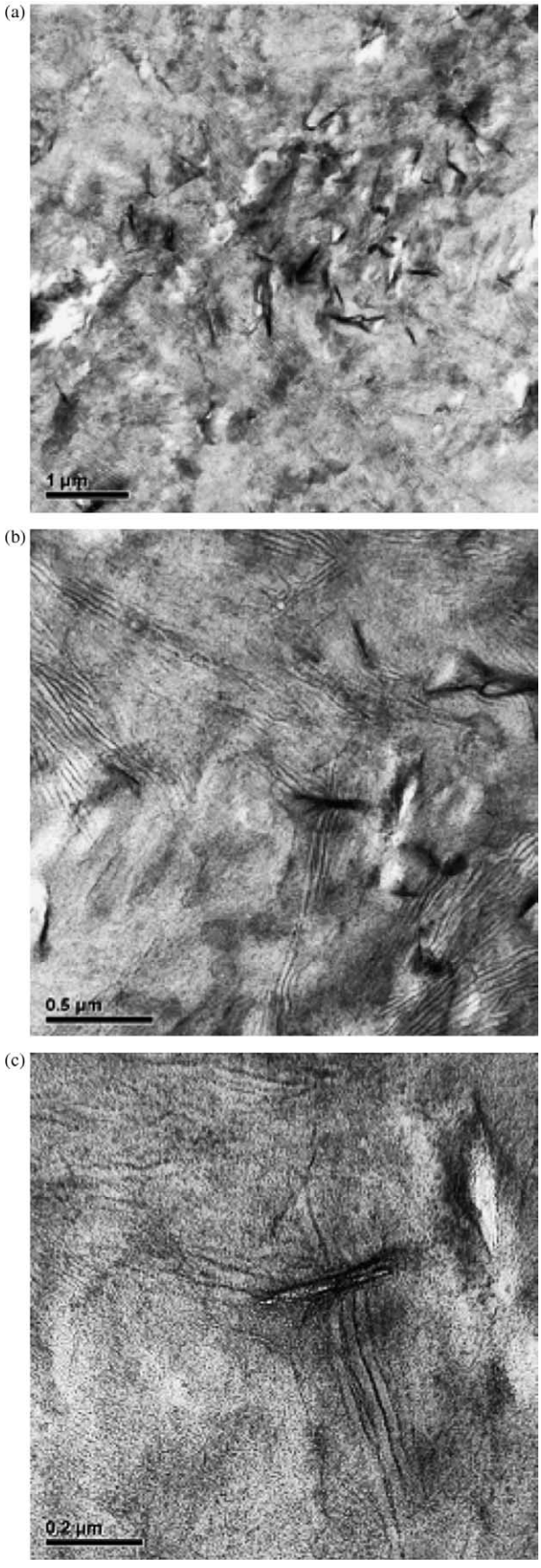

Fig. 8. TEM micrographs of sample PB-M at different magnifications. The metric bar corresponds to (a) 1 μm, (b) 0.5 μm and (c) 0.2 μm.

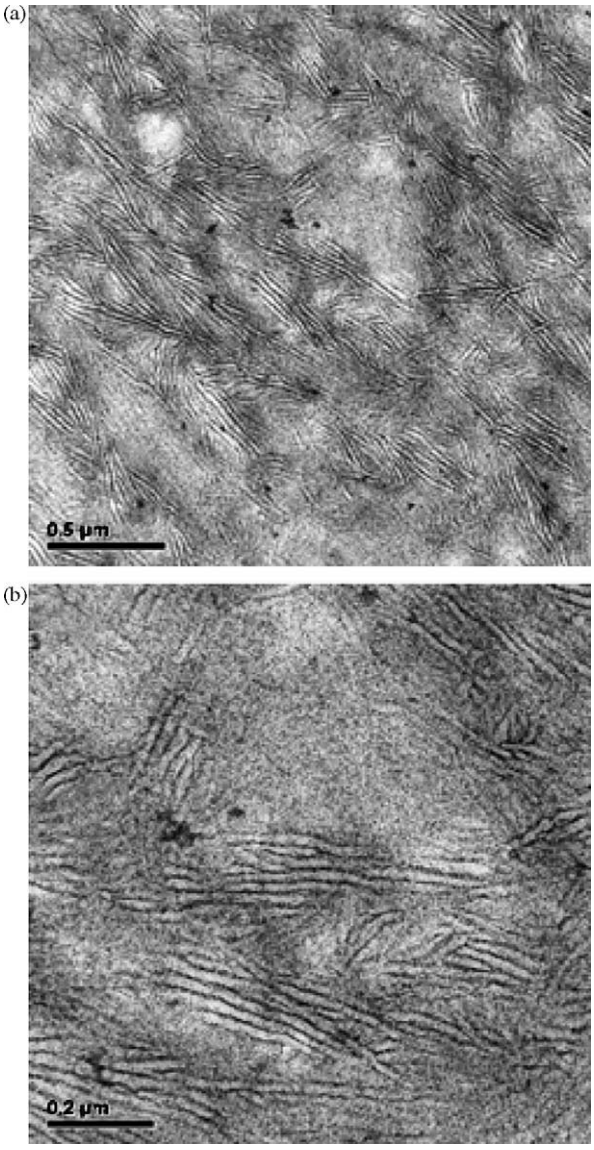

Fig. 9. TEM micrographs of sample PB at different magnifications. The metric bar corresponds to (a) 0.5 μm and (b) 0.2 μm.

In Fig. 8, the morphology of the clay layers can also be studied. No extensive exfoliation occurred, but montmorillonite appears to be homogeneously dispersed in the matrix in the form of small tactoids. SAXS was employed to investigate the morphology of the clay stacks in sample PB-M and in pristine montmorillonite. The SAXS patterns were analyzed by a fitting procedure [14,19] to elucidate the morphology of the lamellar stacks (Fig. 10). The model yielding the best results was that of undistorted lamellar stacks, fitted with a gaussian function. Introduction of the distortion parameter [19] did not allow to accurately fit the experimental pattern. The regular and undistorted nature of clay tactoids can be also noted in TEM micrographs (Fig. 8).

The fitting procedure reproduced SAXS profiles by optimizing the number N of stacked layers, the thickness Z_{clay} of the low-density regions, that indicates how much material is interposed between adjacent clay layers, and the periodicity of the system D_{clay}, along with the relative standard

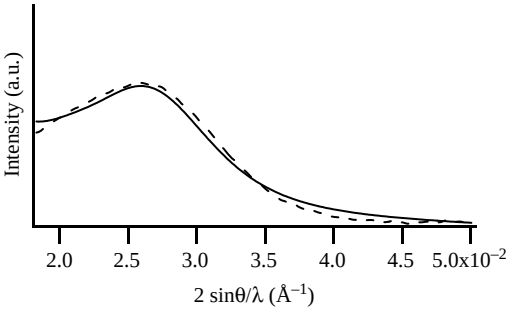

Fig. 10. SAXS pattern of sample PB-M in the clay tactoids' periodicity region. The dashed line represents the experimental data, the solid line represents the fitted ones.

deviations $(\sigma_Z/Z)_{clay}$ and $(\sigma_D/D)_{clay}$. The thickness Y_{clay} of the alumino-silicatic layers was fixed in 10 Å [34]. These structural parameters are shown in Table 2. A shift towards small angles can be observed in the composite, meaning that intercalation occurred. The interlayer spacing expanded 4 Å from pristine clay to the composite. It is very important to observe that the number of layers in the clay tactoids dramatically decreased from a very large number (the model cannot distinguish between structures with more than 50 layers [17]) in pristine clay to just six in the composite. This datum is confirmed by TEM micrographs in which quite thin stacks can be seen. The particular processing conditions adopted were chosen in order to maximize polymer–clay interaction. The elimination of restriction rings in the screw setup was critical to adjust the residence time of the polymer in the extruder and thus to avoid platelet compaction [14]. Most researchers in the field of nanocomposites emphasize the importance of exfoliation in the improvement of physical and mechanical properties. Table 3 shows the mechanical properties and the results of TG analysis. Addition of clay nearly doubled the flexural modulus (MEF). As expected [13], the composite was more rigid than the PB matrix. Along with the property enhancement, a decrease in MFR was observed, as previously reported in the case of analogous polypropylene/nanoclay composites [14]. PB-M also displayed an increase in all the characteristic temperatures obtained by the TG patterns (T_{onset}, T_{offset} and T_{max}), either in nitrogen and air atmosphere, with respect to PB. This confirms that montmorillonite acts as a thermal stabilizer in the composite. Moreover, the degradation of PB-M was remarkably faster than that of PB, as can be noted from the span between T_{onset} and T_{offset}. Even though the results are relative to a single formulation of the system polymer/clay/compatibilizer, it is interesting to note that these significant variations in properties were obtained without extensive exfoliation, but rather by a reduction in the thickness of the clay tactoids down to just six layers on average. This was sufficient to enlarge the interfacial region permitting to exploit the excellent mechanical properties of the clay layers [35–37].

Table 2
Average number of layers (N), thickness of low-density region (Z_{clay}), periodicity of the layers (D_{clay}), thickness distribution values, $(\sigma_Z/Z)_{clay}$ and $(\sigma_D/D)_{clay}$, in the clay tactoids of pristine montmorillonite and of sample PB-M

	N	Z_{clay} (Å)	D_{clay} (Å)	$(\sigma_Z/Z)_{clay}$	$(\sigma_D/D)_{clay}$
Pristine montmorillonite	>50	19	29	0.40	0.30
PB-M	6	23	33	0.35	0.26

Table 3
Mechanical and thermal degradation properties of the examined samples

Test	PB	PB-M
Melt flow rate (g/10 min)	11	8.3
Izod impact resistance @ 23 °C (kJ/m^2)	32.2±4.4	10.7±0.7
Flexural modulus (MPa)	495±18	907±26
Stress at break (MPa)	27.1±0.6	23.0±0.3
Elongation at break (%)	90±6	37±6
T_{onset} in N_2 (°C)	389.7	441.8
T_{max} in N_2 (°C)	439.6	454.9
T_{offset} in N_2 (°C)	455.6	459.9
T_{onset} in air (°C)	318.2	395.7
T_{max} in air (°C)	368.4	421.8
T_{offset} in air (°C)	392.6	426.2

4. Conclusions

The structure, morphology and properties of a polybutene/montmorillonite nanocomposite were investigated. Although the study was limited to one particular formulation of the nanocomposite system, interesting data were nevertheless observed. Nanoclay was found to hinder the attainment of an ordered structure, dramatically increasing the extent and kinetics of the II→I phase transition. A significant improvement of some physical and mechanical properties was obtained without exfoliation of the filler, but only by a reduction in the size of the tactoids and by a slight intercalation. The preparation of polybutene-based nanocomposites could give an impulse to the commercial exploitation of this polymer, not only because it is a way to enhance its already remarkable properties, but also because the aging time necessary to obtain phase I, the most interesting for applicative purposes, is considerably shortened. If compared with polypropylene (PP)-based nanocomposites [14], those based on polybutene exhibit superior performance improvement (for example, clay increased MEF by 50% in PP-based composites, but this parameter doubled when PB was employed) and an easier dispersion of the filler in the matrix, probably due to a better compatibility of the organoclay with the PB chains.

Acknowledgements

The authors thank Dr Thomas Frechen from GKP/P, BASF Aktiengesellschaft for TEM analyses. V.C. gratefully acknowledges financial support by Basell Italia S.p.A., through a Federchimica grant, and the University of Padova. This work was carried out in the context of the European Network of Excellence Nanofun-Poly.

References

[1] Natta G, Corradini P, Danusso F, Mantica E, Mazzanti G, Pino P, et al. J Am Chem Soc 1955;77:1708.

[2] Turner Jones A. Polym Lett 1963;1:455.
[3] Aronne A, Napolitano R, Pirozzi B. Eur Polym J 1986;22:703.
[4] Marigo A, Marega C, Cecchin G, Collina G, Ferrara G. Eur Polym J 2000; 36:131.
[5] Azzurri F, Flores A, Alfonso GC, Baltá Calleja FJ. Macromolecules 2002; 35:9069.
[6] Azzurri F, Flores A, Alfonso GC, Sics I, Hsiao BS, Baltá Calleja FJ. Polymer 2003;44:1641.
[7] Nakafuku C, Miyaki T. Polymer 1983;24:141.
[8] Boor JJ, Mitchell JC. J Polym Sci 1963;A1:59.
[9] Alfonso GC, Azzurri F, Castellano M. J Therm Anal Cal 2001;66:197.
[10] Kaszonyiova M, Rybnikar F, Geil PH. J Macromol Sci Phys 2004;B43: 1095.
[11] Wanjale SD, Jog JP. J Macromol Sci Phys 2003;B42:1141.
[12] Wanjale SD, Jog JP. J Polym Sci Polym Phys Ed 2003;41:1014.
[13] Nathani H, Dasari A, Misra RDK. Acta Mater 2004;52:3217.
[14] Benetti EM, Causin V, Marega C, Marigo A, Ferrara G, Ferraro A, et al. Polymer 2005;46:8275.
[15] Hindeleh AM, Johnson DJ. J Phys D: Appl Phys 1971;4:259.
[16] Vonk CG. Synthetic polymers in the solid state. In: Glatter O, Kratky O, editors. Small angle X-ray scattering. London: Academic Press; 1982. p. 433.
[17] Marega C, Marigo A, Cingano G, Zannetti R, Paganetto G. Polymer 1996; 37:5549.
[18] Hosemann R, Bagchi SN. Direct analysis of diffraction by matter. Amsterdam: North Holland; 1962.
[19] Causin V, Marega C, Marigo A, Ferrara G. Polymer 2005;46:9533.
[20] Azzurri F, Alfonso GC, Gómez MA, Martì MC, Ellis G, Marco C. Macromolecules 2004;37:3755.
[21] Azzurri F, Gómez MA, Alfonso GC, Ellis G, Marco C. J Macromol Sci Phys 2004;B43:177.
[22] Deveaux E, Bourbigot S, El Achari A. J Appl Polym Sci 2002;86:2416.
[23] Ma J, Zhang S, Qi Z, Li G, Hu L. J Appl Polym Sci 2002;86:1978.
[24] Maiti P, Nam PH, Okamoto M, Hasegawa N, Usuki A. Macromolecules 2002;35:2042.
[25] Hambir S, Bulakh N, Jog JP. Polym Eng Sci 2002;42:1800.
[26] Lincoln DM, Vaia RA, Krishnamoorti R. Macromolecules 2004;37: 4554.
[27] Lincoln DM, Vaia RA, Wang Z-G, Hsiao BS, Krishnamoorti R. Polymer 2001;42:9975.
[28] Zannetti R, Manaresi P, Buzzoni GC. Chim Ind (Milan) 1961;43:735.
[29] Asada T, Sasada S, Onogi S. Polym J 1972;3:350.
[30] Bocchini S, Frache A, Camino G, Ferrara G, Fantinel F. Polym Adv Tech 2006;17:246.
[31] Kaszonyiova M, Rybnikar F, Geil PH. J Macromol Sci Phys 2005;B44: 377.
[32] Hackett E, Manias E, Giannelis EP. Chem Mater 2000;12:2161.
[33] Gohil RM, Miles MJ, Petermann J. J Macromol Sci Phys 1982;B21:189.
[34] Shao W, Wang Q, Ma H. Polym Int 2005;54:336.
[35] Vaia RA, Wagner HD. Mater Today 2004;7(11):32.
[36] Pukánszky B. Eur Polym J 2005;41:645.
[37] Eastwood E, Viswanathan S, O'Brien CP, Kumar D, Dadmun MD. Polymer 2005;46:3957.